Proc. 2nd ESIS TC4 Conference on Polymers and Composites, in press, 1999

FRACTURE MECHANICS OF COMPOSITES WITH RESIDUAL STRESSES, TRACTION-LOADED CRACKS, AND IMPERFECT INTERFACES

J. A. NAIRN
Material Science and Engineering, University of Utah, Salt Lake City, Utah 84112, USA

ABSTRACT

By partitioning the total stresses in a damaged composite into either mechanical and residual stresses or into initial and perturbation stresses, it was possible to derive several exact results for the energy release rate due to crack growth. These general results automatically include the effects of residual stresses, traction-loaded cracks, and imperfect interfaces. By considering approximate solutions based on admissible stress states and admissible strain states, it was possible to derive rigorous upper and lower bounds to the energy release rate for crack growth. Two examples of using these equations are mode I fracture in adhesive double cantilever beam specimens and analysis of microcracking in composite laminates.

KEYWORDS

Fracture Mechanics, Energy Release Rate, Residual Stresses, Adhesive Fracture, Matrix Microcracking

INTRODUCTION

Composite materials, especially composites reinforced with aligned, high-modulus fibers, are often very close to being linear elastic up to failure. For this reason, many composite fracture models for composites have been developed using linear-elastic fracture mechanics [1, 2]. Although stress intensity methods from linear-elastic fracture mechanics are not particularly useful for composites, it is often possible to predict composite fracture using energy release rate. In energy based fracture mechanics, it is assumed that cracks propagate when that energy release rate exceeds the fracture toughness of the composite. The required energy release rate can be calculated from a global energy balance using

$$G = -\frac{d\Pi}{dA} = \frac{d(W-U)}{dA} \tag{1}$$

where Π is thermoelastic potential energy, W is external work, U is thermoelastic internal energy, and dA is an increment in total crack area. [3].

The goal of this paper is to apply Eq. (1) to general composite fracture problems when the composite is assumed to be a linear thermoelastic material. There are important effects in heterogeneous composites that make fracture mechanics of composites more difficult than the corresponding analysis for

homogeneous materials. First, because composites are made of phases with disparate thermal expansion coefficients, the phases will inevitably be subjected to residual stresses [4]. These residual stresses can contribute to energy release rate and should be part of every composite fracture model [5]. Second, the heterogeneity of composites sometimes causes cracks to divert in directions that would not be observed in homogeneous materials. If such structure-controlled crack growth results in crack surfaces that contact each other, there may be crack surface tractions. When traction-loaded crack surfaces slide relative to each other during crack growth, that sliding can affect the energy release rate. Third, there will always be interfaces between phases. If these interfaces are not perfect, they may slide relative to each other during crack growth [6]. Like sliding, traction-loaded cracks, sliding, imperfect interfaces can affect the energy release rate. This paper presents some recent fracture mechanics theorems for composites that account for all effects cited above. The **Examples** section applies some of these theorems to analysis of the residual stress effects in adhesive double cantilever beam specimens and to an analysis of matrix microcracking in composite laminates.

FRACTURE MECHANICS THEOREMS

Consider an arbitrary composite subjected to a uniform temperature change of ΔT and to any mixed traction and displacement boundary conditions as illustrated in Fig. 1. The boundary surface S_T is subjected to tractions while the boundary S_u is subjected to to displacement boundary conditions. Let the interior of the composite contain cracks and interfaces and denote the total surface area of cracks and interfaces as S_c. Both cracks and imperfect interfaces [6] can be modeled as 2D surfaces with continuous stresses but possibly discontinuous displacements [7]. When there are traction loads on cracks, an additional boundary condition on S_c is

$$\vec{T} = \vec{T}_c \quad \text{on} \quad S_c \tag{2}$$

where $\vec{T}_c$ includes traction loads on any cracks or tractions induced at sliding interfaces. The goal of this section is derive exact and variational theorems for the energy release rate due to an increase in total crack area for the arbitrary composite in Fig. 1. An increase in crack area corresponds to an increase in the internal area S_c.

Mechanical and Residual Stresses

The full thermal elasticity problem can be treated as a superposition of two problems — one for mechanically applied stresses and one for residual stresses [5, 7]. By partitioning the total stresses into mechanical stresses, $\boldsymbol{\sigma}^m$, and residual stresses, $\boldsymbol{\sigma}^r$, substituting the partitioned stresses into Eq. (1) and making use of virtual work and divergence theorems (the details are in Ref. [7]), it was possible to derive the first energy release rate theorem:

$$G = G_{mech} + \frac{V\Delta T}{2}\left(2\frac{d\left\langle \boldsymbol{\sigma}^m\cdot\boldsymbol{\alpha}\right\rangle}{dA} + \frac{d\left\langle \boldsymbol{\sigma}^r\cdot\boldsymbol{\alpha}\right\rangle}{dA}\right) + \frac{d}{dA}\left(\int_{S_c}\vec{T}^{\,r}\cdot\vec{u}^{\,m}dS + \frac{1}{2}\int_{S_c}\vec{T}^{\,r}\cdot\vec{u}^{\,r}dS\right) \tag{3}$$

where G_{mech} is the mechanical energy release rate or the energy release rate when $\Delta T = 0$:

$$G_{mech} = \frac{d}{dA}\left(\frac{1}{2}\int_{S_T}\vec{T}^{\,0}\cdot\vec{u}^{\,m}dS - \frac{1}{2}\int_{S_u}\vec{T}^{\,m}\cdot\vec{u}^{\,0}dS + \frac{1}{2}\int_{S_c}\vec{T}^{\,m}\cdot\vec{u}^{\,m}dS\right) \tag{4}$$

and angle brackets indicates a volume-averaged quantity over total volume V of the composite:

$$\langle f(x,y,z)\rangle = \frac{1}{V}\int_V f(x,y,z)dV \tag{5}$$

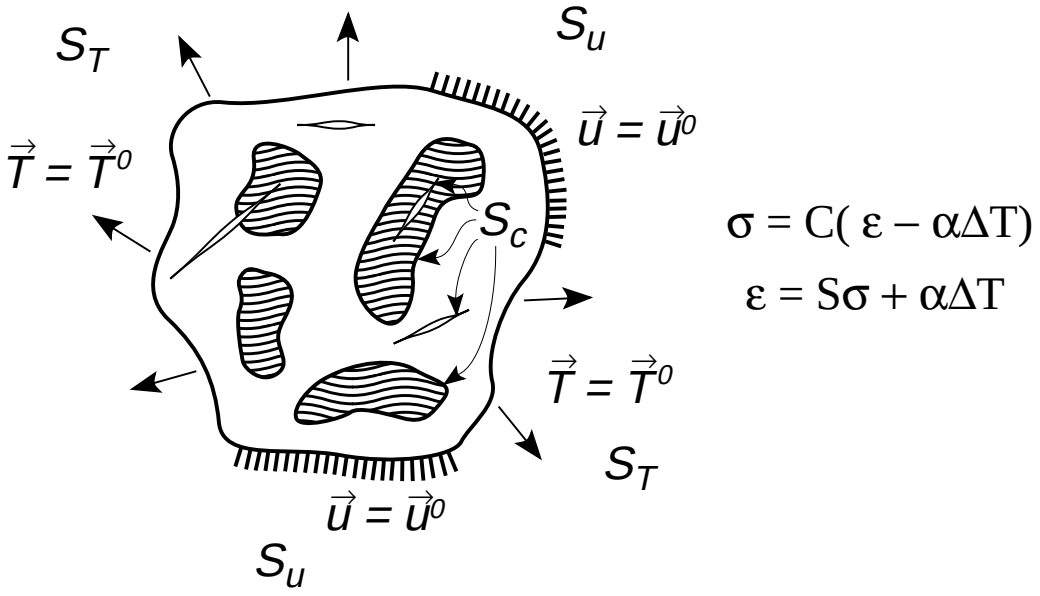

Fig. 1. An arbitrary multiphase material subjected to traction and displacement boundary conditions and containing cracks and interfaces.

Here $\vec{T}$ and u refer to surface tractions and displacements, superscripts m and r refer to mechanical or residual stress terms, and $\boldsymbol{\alpha}$ is the position-sensitive thermal expansion coefficient of the composite. Equation (3) is exact. The first term is the traditional energy release rate. The subsequent terms are required in many composite fracture problems to account for effects of residual stresses, traction-loaded cracks, and imperfect interfaces.

For pure mode I fracture, G is proportional to K_I^2 (stress intensity factor). By Eq. (3), G is quadratic in P and ΔT, but K_I (proportional to a stress) must be linear in P and ΔT. Using these facts, it is possible to simplify G for pure mode I fracture with traction-free cracks and imperfect interfaces to [5]:

$$\frac{G_I}{G_{mech}} = \left(1 + \frac{V\Delta T}{2G_{mech}} \frac{d\left\langle \boldsymbol{\sigma}^m \cdot \boldsymbol{\alpha} \right\rangle}{dA}\right)^2 \tag{6}$$

Notice that the thermoelastic G_I can be calculated from the mechanical stresses alone. There is no need to do thermoelasticity analysis. A similar result in Ref. [7] extends Eq. (6) to include traction-loaded cracks and imperfect interfaces.

Initial and Perturbation Stresses

Alternatively, the full thermal elasticity problem can be partitioned into *initial* and *perturbation* stresses. The initial stresses are the stress prior to crack growth and the perturbation stresses are the *change* in stresses caused by new crack area of size dA. By substituting initial and perturbation stresses into Eq. (1) and making use of virtual work and divergence theorems (the details are in Ref. [7]), it is possible to derive a second energy release rate theorem expressed three different ways:

$$\begin{aligned} G &= \frac{d}{dA}\left(\int_{S_c} \vec{T}^p \cdot \vec{u}^0 dS + \frac{1}{2}\int_{S_c} \vec{T}^p \cdot \vec{u}^p dS\right) \\ &= \frac{d}{dA}\left(\int_{S_c} \vec{T}^p \cdot \vec{u}^0 dS + \frac{1}{2}\int_V \boldsymbol{\sigma}^p \boldsymbol{S} \boldsymbol{\sigma}^p dV\right) = \frac{d}{dA}\left(\int_{S_c} \vec{T}^p \cdot \vec{u}^0 dS + \frac{1}{2}\int_V \boldsymbol{\varepsilon}^p \boldsymbol{C} \boldsymbol{\varepsilon}^p dV\right) \end{aligned} \tag{7}$$

where superscript 0 and p refer to initial and perturbation stresses and $\boldsymbol{S}$ and $\boldsymbol{C}$ are the position-sensitive compliance and stiffness tensors of the composite material. If the initial state corresponds to an *undamaged* composite with perfect interfaces, then the first term in each form of G in Eq. (7) vanishes. In other words, the total energy release rate including residual stresses, traction-loaded cracks, and imperfect interfaces, can be evaluated by finding the change in perturbation stress energy due to formation of damage. Because the perturbation stress analysis is an isothermal ($\Delta T = 0$) stress analysis, the effect of thermal stresses on the energy release rate can be evaluated without any need for a thermoelasticity analysis of the cracked body.

Variational Theorems

In this section, the stresses are again partitioned into initial and perturbation stresses. Assume that the initial stresses are known exactly, but that the perturbation stresses and strains resulting from the formation of a new finite amount a fracture area, ΔA, are only known approximately. Assume further that there are two approximate solutions — one based on an admissible stress field, $\boldsymbol{\sigma}_a^p$, and one based on an admissible strain field, $\boldsymbol{\varepsilon}_a^p$. It has recently been shown [7], that the total energy release rate for formation of the finite fracture area can then be rigorously bounded by

$$-\frac{\Delta\Pi_a}{\Delta A} \le \Delta G \le \frac{\Delta\Gamma_a}{\Delta A} \tag{8}$$

where $\Delta\Gamma_a$ and $\Delta\Pi_a$ are the approximate changes in complementary and potential energy due to any admissible stress or strain states calculated by:

$$\Delta\Gamma_a = \frac{1}{2}\int_V \boldsymbol{\sigma}_a^p \boldsymbol{S} \boldsymbol{\sigma}_a^p dV + \int_{S_c} \vec{T}_a^{\,p} \cdot \vec{u}^{\,0} dS \tag{9}$$

$$\Delta\Pi_a = \frac{1}{2}\int_V \boldsymbol{\varepsilon}_a^p \boldsymbol{C} \boldsymbol{\varepsilon}_a^p dV - \int_{S_c} (\vec{T}_c - \vec{T}_c^{\,0}) \cdot \vec{u}^{\,0} dS - \int_{S_c} (\vec{T}_c - \vec{T}_c^{\,0}) \cdot \vec{u}_a^{\,p} dS \tag{10}$$

In many composite failure analyses, however, the concern is with propagation of damage where neither the initial nor the perturbation stress are known exactly. If the stresses in the undamaged laminate are known exactly, it is still possible to rigorously bound the energy release rate for the propagation of damage from damage area A_1 to damage area A_2 by:

$$-\frac{\Delta\Pi_a(0\to A_2) + \Delta\Gamma_a(0\to A_1)}{A_2 - A_1} \le \Delta G(A_1 \to A_2) \le \frac{\Delta\Gamma_a(0\to A_2) + \Delta\Pi_a(0\to A_1)}{A_2 - A_1} \tag{11}$$

Unless the rigorous bounds for damage initiation (from Eq. (8)) are very tight, the rigorous bounds for damage propagation (from Eq. (11)) are likely to be far apart. Perhaps the rigorous propagation bounds are too pessimistic. Because the admissible stress or strain states each provide approximate solutions, it is possible to define approximate energy release rates derived from each approximate solution using

$$\Delta G_1(A_1 \to A_2) = \frac{\Delta\Gamma_a(0\to A_2) - \Delta\Gamma_a(0\to A_1)}{A_2 - A_1} \tag{12}$$

$$\Delta G_2(A_1 \to A_2) = -\frac{\Delta\Pi_a(0\to A_2) - \Delta\Pi_a(0\to A_1)}{A_2 - A_1} \tag{13}$$

$\Delta G_1(A_1 \to A_2)$ and $\Delta G_2(A_1 \to A_2)$ will, in general, be much closer to each other than the bounds in Eq. (11). Perhaps, therefore, in practice, they will provide tighter, albeit non-rigorous, bounds to $\Delta G(A_1 \to A_2)$. An example of using such *practical* bounds to analyze composite microcracking will be given in the **Examples** section.

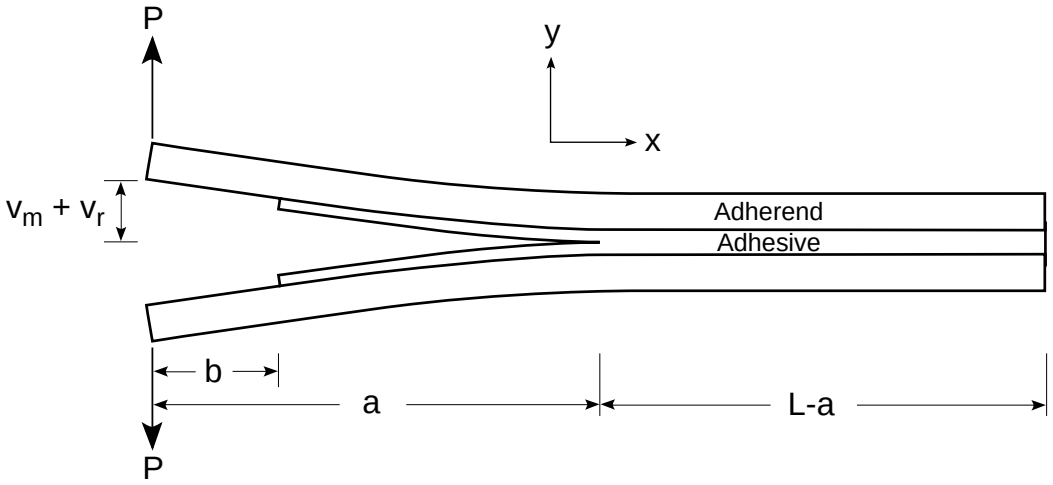

Fig. 2. A double cantilever beam specimen used to measure the mode I toughness of adhesive bonds. The cantilever arm length is a, the total specimen length in L. Sometimes the adhesive does not extend to the end of the arms; here the adhesive stops a distance b from the ends.

EXAMPLES

Adhesive Double Cantilever Beam Specimen

Figure (2) shows a double cantilever beam (DCB) specimen that is often used to measure the mode I fracture toughness of adhesives, G_{Ic}. When the thermal expansion coefficient of the adherend and adhesive are different, such specimens will inevitably have residual stresses. Starting from Eq. (6), it has recently been shown that the total thermoelastic energy release rate for this specimen can be written extremely accurately as [8]:

$$G_I = \left(C_m \left(1 + 1.15\frac{\Delta}{a} \right) Pa + C_r \Delta T \right)^2 \tag{14}$$

where C_m and C_r are mechanical and residual stress terms that can easily be evaluated from simple beam theory and depend only on the effective compliance and thermal curvature properties of each arm of the specimen. The first term in Eq. (14) is the mechanical loading part of G_I. It is known that simple beam theory, by itself, it not sufficiently accurate because of crack-tip rotation effects [9]. Williams [9] has developed a corrected beam theory that improves the mechanical analysis by replacing the actual crack length a by an *effective* crack length $a + \Delta$ where Δ is a function only of beam properties and dimensions [9]. By comparison to numerous finite element results, it was empirically determined that an effective crack length of $a + 1.15\Delta$ (using the Δ from Ref. [9]) improves the results and is extremely accurate for any beam dimensions used in experiments [8]. The second term in Eq. (14) is the residual stress contribution to G_I. In contrast to the mechanical term, the residual stress term can be calculated accurately for any typical beam dimensions by using simple, uncorrected beam theory [8]. It is thus a simple exercise to include residual stress effects in analysis of fracture experiments on adhesive DCB specimens.

Although it is easy to account for residual stresses, most work on adhesives and most standards for characterization of adhesives ignore residual stresses. The questions arises: what is the consequence of ignoring residual stresses? Assume that the *true* toughness of an adhesive is G_{Ic} which implies that failure occurs when $G_I = G_{Ic}$. Using the total energy release rate in Eq. (14), failure will occur at an applied load of

$$P = \frac{\sqrt{G_{Ic}} - C_r \Delta T}{C_m (a + 1.15\Delta)} \tag{15}$$

In work that ignores residual stresses, this P will be the experimentally determined failure load, but the adhesive toughness will be calculated by an analysis that ignores residual stresses. Taking Eq. (14) with $\Delta T = 0$ as an accurate result that ignores residual stresses, such work would arrive at an *apparent* toughness that differs from the *true* toughness, G_{Ic}, by

$$G_{Ic}^{app} = \left(\sqrt{G_{Ic}} - C_r\Delta T\right)^2 \tag{16}$$

Such an apparent toughness can be higher or lower than the true toughness depending on the sign of C_r. For polymeric adhesives between metallic adherends, C_r is always negative which means an apparent toughness measured by ignoring residual stresses will be too high or a non-conservative characterization of the true adhesive properties [8].

The precise magnitude of the errors in G_{Ic}^{app} depends on beam dimensions, adhesive and adherend properties, G_{Ic}, and ΔT. For sample calculations of errors, consider an adhesive with $G_{Ic} = 200$ J/m^2, residual stresses due to $\Delta T = -100$°C, and a thermal expansion mismatch between adherend and adhesive of $\Delta\alpha = -40\times10^{-6}$ K^{-1}. These parameters correspond to a typical high-temperature-cure epoxy adhesive bonded to metallic adherends. Figure (3) plots the percentage error in G_{Ic}^{app} as a function of modulus ratio $R = E_1/E_2$ and layer thickness ratio $\lambda = t_1/t_2$ where subscripts 1 and 2 indicate adherend and adhesive, respectively. The errors are extremely large for low R and low λ and decrease as either R or λ increase. In general, the errors are never insignificant. The dashed vertical line shows a typical R value for aluminum-epoxy specimens ($R = 28$). Despite the high aluminum-epoxy R value, the errors exceed 1% even with a very thin adhesive ($\lambda = 64$). The errors in aluminum-epoxy specimens increase to over 40% as λ decreases to 2, but typical adhesive specimens will have a much larger λ and thus a much smaller error. The nearly-horizontal dashed line gives the errors caused in the mechanical energy release rate when ignoring the crack-length correction term 1.15Δ. The error due to ignoring crack tip rotation are typically similar in magnitude to the errors due to ignoring residual stress. It is common practice to correct adhesive DCB results for crack tip rotation effects. Considering the simplicity of also correcting for residual stresses and the fact that the magnitude of the effects are similar, it should also be common practice to correct adhesive DCB results for residual stress effects.

Laminate Microcracking

When cross-ply laminates ($[0_n/90_m]_s$) are loaded in tension parallel to the 0° plies, the 90° plies develop transverse cracks or matrix microcracks (see review article Ref. [2]). On continued loading, the 90° plies crack into a roughly periodic array of microcracks. For analysis of a microcracked specimen, one can analyze the unit cell of damage containing a single microcrack as illustrated in Fig. 4. Previous work has derived approximate 2D, plane-stress solutions to the stresses in the $x-z$ plane of a microcracked laminate based either on an admissible stress state [10, 11, 12] or an admissible strain state [13]. These two types of solutions, which originally were for traction-only loading, were recently modified slightly to give solutions for constant-displacement boundary conditions that are more appropriate for analysis of experiments run in displacement control [7]. The two modified solutions can be used to bound energy release rate and to analyze experiments.

By using the admissible-stress-state solution to obtain an upper bound and the admissible-strain-state solution to obtain a lower bound, the total energy released upon forming n microcracks (denoted here as $\Delta G_m(0\rightarrow n)$) in a laminate can be rigorously bounded by:

$$t_1\left(\sigma_{xx,1}^0\right)^2\left\langle C_3\frac{E_A^U(\rho_i)}{E_0}\chi_U(\rho_i)\right\rangle \le \Delta G_m(0\rightarrow n) \le t_1\left(\sigma_{xx,1}^0\right)^2\left\langle C_3\frac{E_A^L(\rho_i)}{E_0}\chi_L(\rho_i)\right\rangle \tag{17}$$

where $2t_1$ is the total thickness of the 90° plies, $\sigma_{xx,1}^0$ is the total stress in the 90° plies in the absence of microcracking, $E_A^U(\rho_i)$ and $E_A^L(\rho_i)$ are the upper and lower bound modulus for laminates with periodic

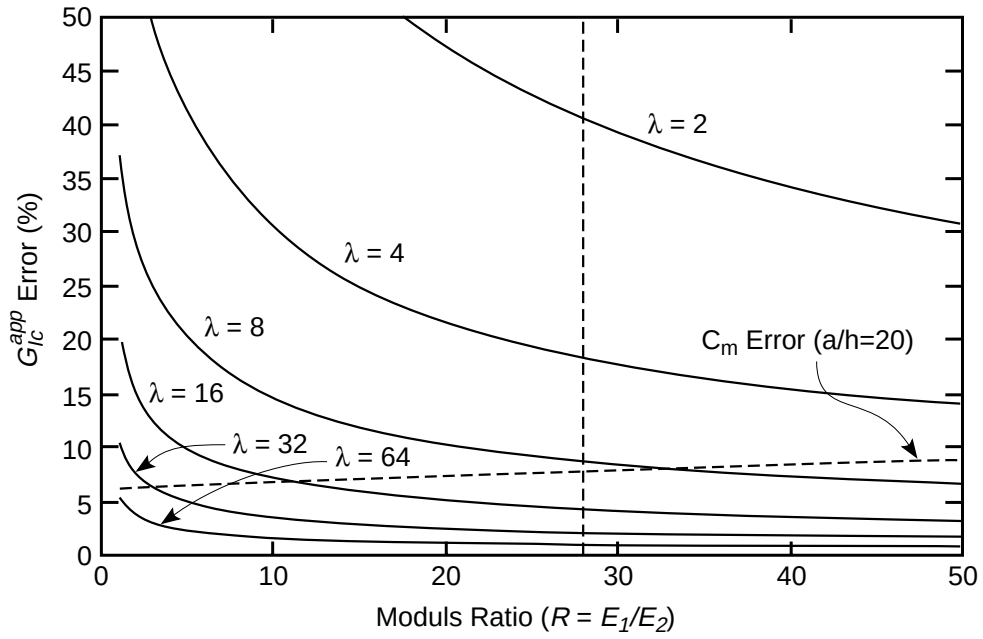

Fig. 3. The error in G_{Ic}^{app} when residual stresses are ignored as a function of modulus ratio R for various values of thickness ratio λ. The adhesive DCB specimens were assumed to have $h = 5$ mm, $G_{Ic} = 200$ J/m^2, $\Delta\alpha = -40 \times 10^{-6}$ K^{-1}, and $\Delta T = -100^{\circ}$C.

microcracks intervals of aspect ratio ρ_i, and $\chi_U(\rho_i)$ and $\chi_L(\rho_i)$ are excess energy functions derived elsewhere [7]. C_3 is a constant that depends only on ply properties and laminate structure. The terms $E_A^U(\rho_i)$ and $\chi_U(\rho_i)$ are derived from the admissible-strain-state solution [7]; the terms $E_A^L(\rho_i)$ and $\chi_L(\rho_i)$ are derived from the admissible-stress-state solution [7].

A sample plot of the rigorous bounds on $\Delta G_m(0 \to n)$ for a $[0/90_2]_s$ E-glass/epoxy laminate is given in Fig. 5. This plot is the total energy released per unit area as a function of crack density for loading conditions giving unit stress in the 90° plies ($\sigma^0_{xx,1} = 1$ MPa). The upper and lower bounds are fairly far apart at low crack density, but get closer at high crack density. These bounds were calculated from Eq. (17) which was derived using displacement boundary conditions [7]; they are appropriate for analysis of experiments in displacement control. In conventional fracture mechanics, which analyzes an infinitesimal amount of crack growth, the energy release rate is independent of load *vs.* displacement boundary conditions. When analyzing discrete amounts of fracture, sometimes termed finite fracture mechanics [14, 15], however, it is important to use the appropriate boundary conditions because the energy released depends on whether the analysis is done for load control or displacement control conditions [7, 15].

The more commonly required energy release rate for analyzing microcracking experiments [2] is the energy release rate for the formation of the next microcrack: $\Delta G_m(n \to n+1)$. The rigorous bounds to $\Delta G_m(n \to n+1)$ can be found from Eq. (11). Alternatively, practical bounds can be found from Eqs. (12) and (13). Using the admissible-stress-state and the admissible-strain-state solution, the practical bounds are:

$$\Delta G_{m1}(n \to n+1) = C_3 t_1 \left(\sigma^0_{xx,1}\right)^2 \left(2\frac{E_A^L(\rho/2)}{E_0}\chi_L(\rho/2) - \frac{E_A^L(\rho)}{E_0}\chi_L(\rho)\right) \tag{18}$$

$$\Delta G_{m2}(n \to n+1) = C_3 t_1 \left(\sigma^0_{xx,1}\right)^2 \left(2\frac{E_A^U(\rho/2)}{E_0}\chi_U(\rho/2) - \frac{E_A^U(\rho)}{E_0}\chi_U(\rho)\right) \tag{19}$$

Figure 6 gives sample calculations for both rigorous and practical bounds to $\Delta G_m(n \to n+1)$ for $[0/90_2]_s$ E-glass/epoxy laminate as a function of crack density for loading conditions giving $\sigma^0_{xx,1} = 1$ MPa. The

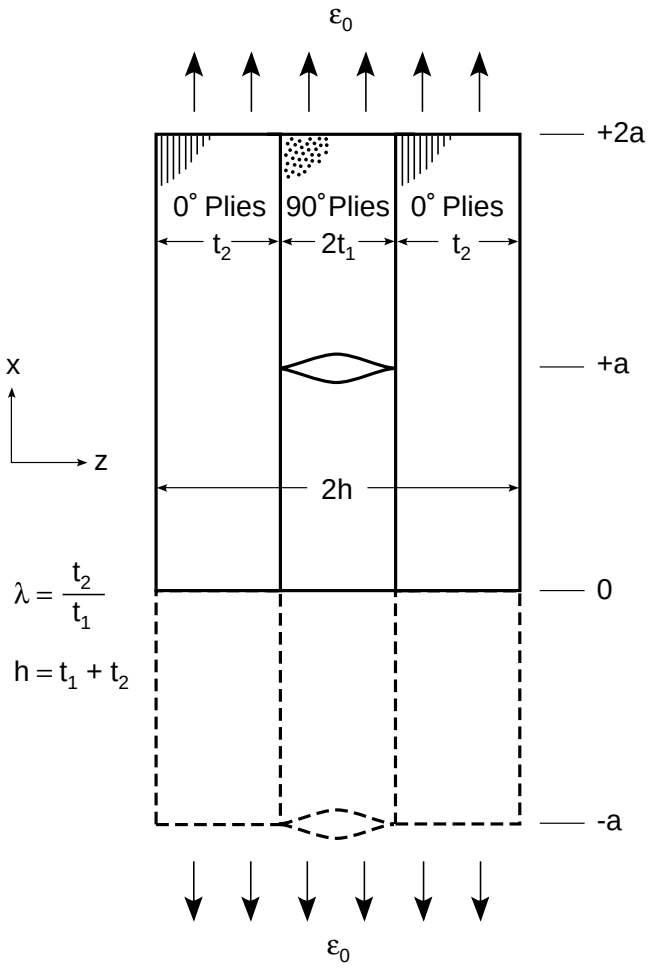

Fig. 4. A unit cell of damage for a $[0_n/90_m]_s$ laminate with a periodic array of microcracks spaced by distance $2a$. This figure is an edge view or x–z plane view. The laminate width direction is in the y direction. The axial load is applied in the x direction.

symbols give some finite element calculations of the energy release rate. The rigorous upper and lower bounds bound the numerical FEA results but are fairly far apart. The practical bounds (ΔG_{m1} and ΔG_{m2}) always bound the numerical results, but the sense of which practical bound is an upper bound and which is a lower bound switches at a crack density of about 0.6 mm^{-1}.

All energy release rates for microcracking can be written in the generic form

$$\Delta G_m(D) = \left(\sigma^0_{xx,1}\right)^2 \Delta G_{m,unit}(D) = \left(k_m\sigma_0 + k_{th}\Delta T\right)^2 \Delta G_{m,unit}(D) \tag{20}$$

where $\Delta G_{m,unit}(D)$ is the energy release rate when there is unit initial stress in the 90° plies and the current microcrack density is D. The second equation expresses $\sigma^0_{xx,1}$ for linear thermoelastic laminates in terms of mechanical and thermal *stiffnesses* which can easily be calculated from laminated plate theory [2, 16]. In finite fracture mechanics analysis of microcracking, it is assumed the next microcrack forms when $\Delta G_m(D) = G_{mc}$ where G_{mc} is the microcracking fracture toughness for the material. Under this assumption, Eq. (20) can be rewritten as

$$-\frac{k_m}{k_{th}}\sigma_0 = -\frac{\sqrt{G_{mc}}}{k_{th}\sqrt{\Delta G_{m,unit}(D)}} + \Delta T \tag{21}$$

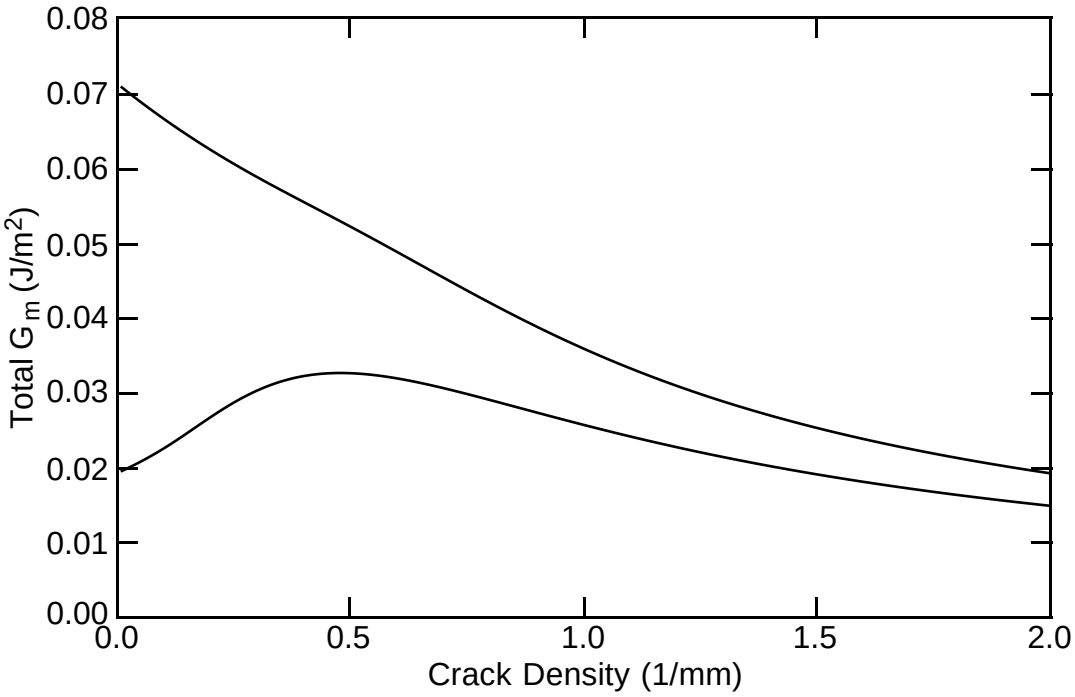

Fig. 5. Rigorous bounds on total energy release rate due to formation of all microcracks under displacement control. The calculations are for a $[0/90_2]_s$ E-glass/epoxy laminate. The assumed laminate properties are in Ref. 13. The calculation is for $\sigma^0_{xx,1} = 1$ MPa.

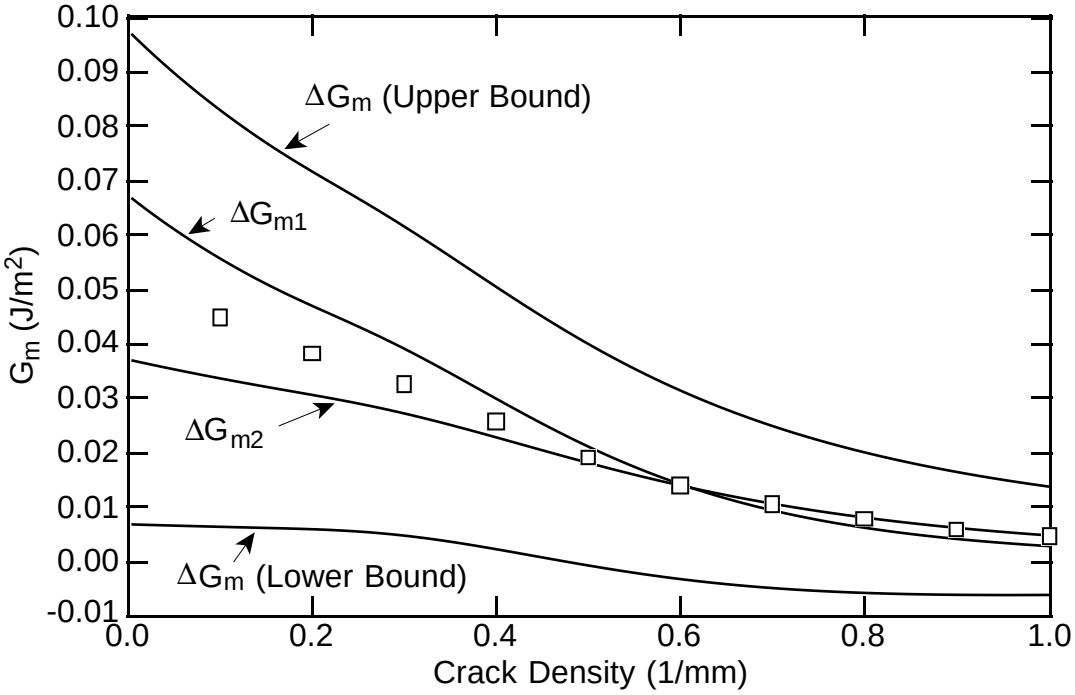

Fig. 6. Rigorous (upper and lower bounds) and practical bounds (ΔG_{m1} and ΔG_{m2}) for the energy release rate $\Delta G_m(n \rightarrow n+1)$ or the energy released due to the formation of the next microcrack. The calculations are for a $[0/90_2]_s$ E-glass/epoxy laminate. The assumed laminate properties are in Ref. 13. The calculation is for $\sigma^0_{xx,1} = 1$ MPa. The symbols are finite element analysis calculations for $\Delta G_m(n \rightarrow n+1)$.

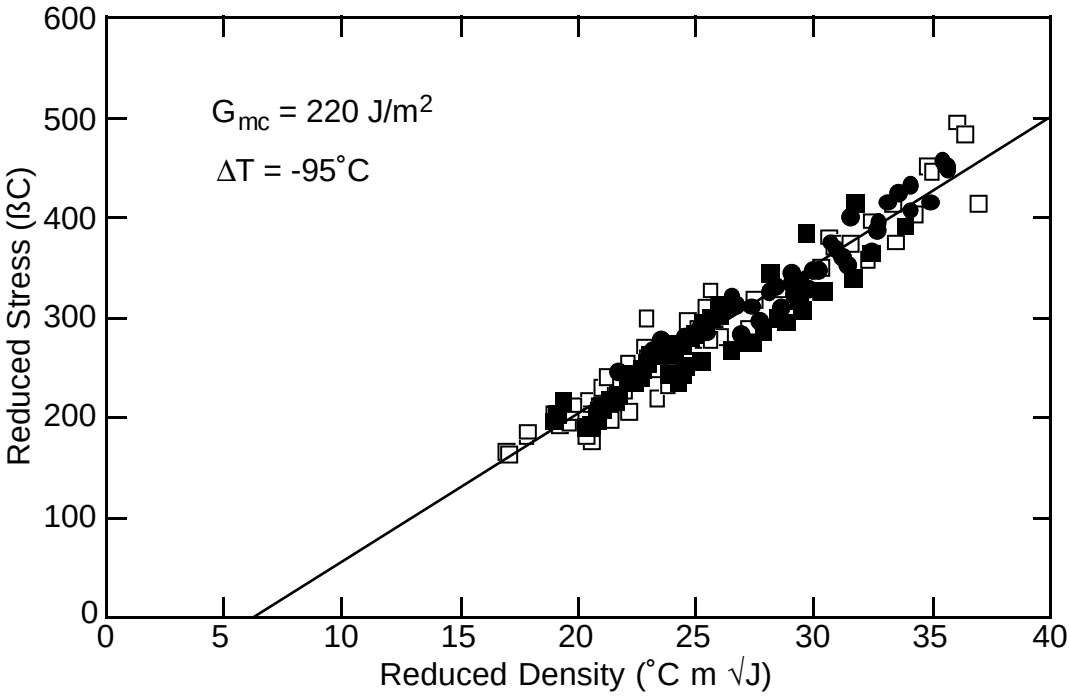

Fig. 7. Master plot analysis for 14 $[0_n/90_m]_s$ (open symbols) and $[90_m/0_n]_s$ (filled symbols) AS4/3501-6 carbon/epoxy laminates. $G_{m,unit}(D)$ was calculated from a complementary energy analysis with constant displacement boundary conditions. The straight line is a linear fit to the experimental results. The slope and intercept of the fit give $G_{mc} = 220$ J/m^2 and $\Delta T = -95$°C.

This equation suggests defining a *reduced* stress, σ_R, and *reduced* crack density, D_R, by

$$\sigma_R = -\frac{k_m}{k_{th}}\sigma_0 \qquad \text{and} \qquad D_R = -\frac{1}{k_{th}\sqrt{\Delta G_{m,unit}(D)}} \tag{22}$$

which are related by

$$\sigma_R = D_R\sqrt{G_{mc}} + \Delta T \tag{23}$$

By Eq. (23), a plot of σ_R as a function of D_R should be linear with a slope of $\sqrt{G_{mc}}$ and an intercept of ΔT. Because G_{mc} and ΔT should be independent of laminate geometry, the results from all laminates should all fall on the same line which defines a master plot for that material

The construction of a master plot requires a result for $\Delta G_{m,unit}(D)$. As seen in Fig. 6 the practical bounds give very accurate results for the energy released due to the formation of the microcrack. Figure 7 gives a master plot for 14 different laminates of AS4/3501-6 carbon/epoxy laminates with $\Delta G_{m,unit}(D)$ calculated using the practical bound $\Delta G_{m1}(n \to n+1)$. The data from all laminates fall on a single linear master plot. The slope gives the toughness as $G_{mc} = 220$ J/m^2 and the residual stress term as $\Delta T = -95$°C. Notice that the microcracking fracture process is sensitive to residual stresses and thus residual stresses must be included to analyze the experiments correctly. Fortunately, however, the residual stresses do not need to be measured; they are determined automatically as the intercept of the linear master plot. The success of the master plot analysis is experimental verification of two points. First, it shows that the finite fracture mechanics criterion that microcracks form when $\Delta G_m(D) = G_{mc}$ is an appropriate failure criterion for predicting microcracking. Attempts to use other failure criteria, such as strength-based methods, give very poor master plots [16]. Second, it shows that the practical bound $\Delta G_{m1}(n \to n+1)$ is sufficiently accurate for analyzing microcracking experiments. Attempts to use less accurate energy release rate analyses gave worse master plots [15, 16]. Attempts to use more accurate energy release rate analyses are not likely to yield much improvement because Fig. 7 is probably already as narrow as possible when considering experimental scatter in fracture experiments.

CONCLUSIONS

The key results of this paper are to express energy release rates for composite fracture in several alternate forms. All of these forms are mathematically identical, but specific forms will be more convenient than others for specific composite fracture problems. Equation (3) gives G in terms of mechanical and residual stresses. Equation (6) gives a special case of Eq. (3) for mode I crack growth. Equation (7) gives G in terms of initial and perturbation stresses. Equations (8) and (11) give variational bounds to ΔG. Each of these results includes residual stresses, traction-loaded cracks, and imperfect interfaces. Most of the equations simplify further when all cracks are traction free and there is no sliding at imperfect interfaces.

ACKNOWLEDGMENTS

This work was supported, in part, by a grant from the Mechanics of Materials program at the National Science Foundation (CMS-9713356), and, in part, by the University of Utah Center for the Simulation of Accidental Fires and Explosions (C-SAFE), funded by the Department of Energy, Lawrence Livermore National Laboratory, under Subcontract B341493.

REFERENCES

1. Hashemi, S., Kinloch, A. J. and Williams, J. G. (1990) *Proceedings of the Royal Society of London* **A347**, 173.
2. Nairn, J. A.and Hu, S. (1994). In: *Damage Mechanics of Composite Materials*, R. Talreja (Ed.). Elsevier, Amsterdam, pp. 187–243.
3. Williams, J. G. (1984). *Fracture Mechanics of Solids*, John Wiley & Sons, New York.
4. Nairn, J. A. and Zoller, P. (1985) *Journal of Material Science* **20**, 355.
5. Nairn, J. A. (1997) *Journal of Applied Mechanics* **64**, 804.
6. Hashin, Z. (1990) *Mechanics of Materials* **8**, 333.
7. Nairn, J. A.(2000) *Int. J. Fracture*, in press.
8. Nairn, J. A. (2000) *Int. J. Adhesion & Adhesives* **20**, 59.
9. Williams, J. G. (1995). In *Proc. Int'l Mechanical Engineering Congress and Exhibition: The Winter Annual Meeting of the ASME, Symposium on Mechanics of Plastics and Plastic Composites*, 12-17 November 1995, San Francisco, USA.
10. Hashin, Z. (1985) *Mechanics of Materials* **4**, 121.
11. Nairn, J. A. (1989) *Journal of Composite Materials* **23**, 1106. (and errata: *(1990) Journal of Composite Materials* **24** 233).
12. Varna, J. and Berglund, L. A. (1992) *Journal of Reinforced Plastics and Composites* **11**, 708.
13. Nairn, J. A. (1995) *Proceedings of the* 10^{th} *International Conference on Composite Materials* **I**, 423.
14. Hashin, Z. (1996) *Journal of the Mechanics and Physics of Solids* **44**, 1129.
15. Nairn, J. A. (1999) *Fifth Int'l Conf. on Deformation and Fracture of Composites*, 1.
16. Nairn, J. A., S. Hu, and J. S. Bark (1993) *Journal of Material Science* **28**, 5099.